Radiol Phys Technol (2015) 8:295–304
DOI 10.1007/s12194-015-0320-7

Iterative image reconstruction that includes a total variation regularization for radial MRI

Shinya Kojima[1] · Hiroyuki Shinohara[2] · Takeyuki Hashimoto[3] · Masami Hirata[1] · Eiko Ueno[1]

Received: 9 February 2015 / Revised: 8 May 2015 / Accepted: 11 May 2015 / Published online: 20 May 2015

Abstract This paper presents an iterative image reconstruction method for radial encodings in MRI based on a total variation (TV) regularization. The algebraic reconstruction method combined with total variation regularization (ART_TV) is implemented with a regularization parameter specifying the weight of the TV term in the optimization process. We used numerical simulations of a Shepp–Logan phantom, as well as experimental imaging of a phantom that included a rectangular-wave chart, to evaluate the performance of ART_TV, and to compare it with that of the Fourier transform (FT) method. The trade-off between spatial resolution and signal-to-noise ratio (SNR) was investigated for different values of the regularization parameter by experiments on a phantom and a commercially available MRI system. ART_TV was inferior to the FT with respect to the evaluation of the modulation transfer function (MTF), especially at high frequencies; however, it outperformed the FT with regard to the SNR. In accordance with the results of SNR measurement, visual impression suggested that the image quality of ART_TV was better than that of the FT for reconstruction of a noisy image of a kiwi fruit. In conclusion, ART_TV provides radial MRI with improved image quality for low-SNR data; however, the regularization parameter in ART_TV is a critical factor for obtaining improvement over the FT.

Keywords Radial MRI · Total variation · Inverse problem · Iterative reconstruction · Algebraic reconstruction

1 Introduction

In MRI, the Cartesian scan is the most common technique used for the trajectory of k-space. On the other hand, a radial scan is frequently employed; it fills the k-space radially. Because the radial scan collects data densely at the center of k-space, it is relatively insensitive to motion artifacts [1–4]. Furthermore, an aliasing artifact is not caused in the radial scan [5, 6] and thus it can be applied to cardiac MRI [7–11]. By use of a small field of view (FOV), a high-resolution image can be obtained with the radial scan; however, the signal-to-noise ratio (SNR) is decreased. A conventional image reconstruction for radial encodings in MRI uses the Fourier transform (FT). A rearrangement of the polar coordinate data to a rectangular grid is required for that reconstruction [1, 3, 12]. However, the rearrangement of the coordinates is not performed when a projection reconstruction such as the filtered back-projection method is employed for image reconstruction [4, 13]. Recently, iterative image reconstruction has been employed in radial MRI [14–16]. Iterative image reconstruction has an affinity for the radial scan, because it does not require rearrangement of k-space data. In addition, it can perform the reconstruction by incorporating various techniques, such as a noise reduction that is effective for low-SNR images [16].

✉ Shinya Kojima
yancy123xyz@gmail.com

[1] Department of Radiology, Tokyo Women's Medical University Medical Center East, 2-1-10 Arakawa-ku, Tokyo, Japan

[2] Tokyo Metropolitan University, 7-2-10 Arakawa-ku, Tokyo, Japan

[3] Faculty of Childhood Education, Yokohama Soei University, 1 Miho-cho, Midori-ku, Yokohama, Kanagawa, Japan

Total variation (TV), initially presented by Radin et al. [17], is used in image processing for reducing noise and blur in images while preserving sharp edges. The basic assumption of TV is that the object consists of areas with constant (or only mildly varying) intensity; this assumption applies quite well to tomographic images [14]. Image reconstruction with TV has produced feasible images from a reduced number of projections in clinic. Sidky et al. [18] studied the algebraic reconstruction method with TV regularization for few-view and limited-angle data in divergent-beam CT. Block et al. [14] reported on the conjugate gradient method with TV regularization for undersampled radial MRI and compared it with the FT method, showing that the former is superior to the latter with regard to reconstructed image quality. Block et al. performed pioneering work in the application of TV to radial MRI, but their results were mainly concerned with the visual impression of the spatial resolution and artifacts of the reconstructed images. Quantitative evaluations that include the spatial resolution and SNR have not been reported. Therefore, it is as yet not certain whether iterative image reconstruction regularized with TV can be applied not only to undersampled radial MRI, but also to conventional radial MRI (without undersampling). In the present work, the algebraic reconstruction method with total variation regularization was implemented for conventional radial MRI sampling with low-SNR data, and the quality of the reconstructions was investigated quantitatively.

2 Materials and methods

In the rest of this work, algebraic reconstruction with TV regularization is referred to as ART_TV. First, we used ART_TV on computer-simulated data to carry out a fundamental investigation. Next, we examined experimental data from a commercially available MRI system. A 1.5-T MRI system (Magnetom Avanto, Siemens Medical Solutions, Erlangen, Germany) was employed. In addition, the reconstructed images from ART_TV were compared with those from the FT. The computer simulations and the image reconstruction were carried out with use of a program written in C++ (Visual Studio 2010, Microsoft Corporation, Redmond, Washington, USA), on a computer equipped with an Intel 2.0 GHz processor and with 8 GB of RAM.

2.1 Algebraic reconstruction method based on total variation regularization

We expressed the gradient of image f as $\nabla f(i,j)$, where each pixel with indices (i, j),

$$\nabla f(i,j) = \sqrt{\left(\frac{\partial f}{\partial i}\right)^2 + \left(\frac{\partial f}{\partial j}\right)^2}. \tag{1}$$

The total variation (TV) of the image, denoted as $\|f\|_{TV}$, is the L_1 norm of gradient $\nabla f(i,j)$, where the L_1 norm of vector f is defined by Eq. (2):

$$\|f\|_1 = \sum_{i,j=1}^{n} |f_{i,j}| = |f_{1,1}| + |f_{1,2}| + \cdots + |f_{n,n-1}| + |f_{n,n}|. \tag{2}$$

$\|f\|_{TV}$ is given numerically in Eq. (3):

$$\|f\|_{TV} = \sum_{i,j} \nabla f(i,j) = \sum_{i,j} \sqrt{(f_{i,j} - f_{i-1,j})^2 + (f_{i,j} - f_{i,j-1})^2}. \tag{3}$$

The projection data for the object were obtained by inverse FT of radial MRI encodings with complex data, and the reconstruction was performed to minimize the total variation, expressed as

$$\text{Minimize } \|f\|_{TV} \qquad \text{subject to} \quad Cf = y, \tag{4}$$

where f is the reconstructed image with N^2 dimensions ($N = 256$), y is the projection data (sinogram) with N^2 dimensions, and C is the system matrix with N^4 dimensions.

TV is the measure of the total variation of the image, and its use enforces a nearly flat image with the gradient being zero in most area [19, 20]. The resultant image tends to be piecewise constant. The fidelity between the reconstructed image and the projection data in Eq. (4) is increased by iterative changes when using the algebraic reconstruction technique (ART). These changes are expressed as

$$f^{k,m+1} = f^{k,m} + C^T \frac{(y - Cf^{k,m})}{C^T C}, \tag{5}$$

with C^T being the transpose of the system matrix and $f^{k,m}$ being the image at the mth subiteration within the kth iteration. Minimization of the total variation of the update of image in Eq. (5) is done by use of the gradient-descent algorithm expressed as

$$f_{\mathrm{TV}}^{k,m+1} = f^{k,m+1} - \beta \nabla \left\| f^{k,m+1} \right\|_{\mathrm{TV}}, \tag{6}$$

where $\nabla \left\| f^{k,m+1} \right\|_{\mathrm{TV}}$ is the partial derivative of $\left\| f^{k,m+1} \right\|_{\mathrm{TV}}$. β is the regularization parameter that specifies the weight of TV at the $m + 1$th subiteration within the kth iteration. We chose to look at $\beta = 0.01$, 0.1, and 1 % of the maximum signal intensity of the updated image at the $m + 1$th subiteration within the kth iteration. In practice, a small number ε that is 1×10^{-4} is necessary for calculation of

the partial derivative in Eq. (6) so that the L_1 norm is differentiable [18]:

$$\nabla \left\| f^{k,m+1} \right\|_{\mathrm{TV}} \cong \frac{f_{i,j} - f_{i-1,j}}{\sqrt{\left(f_{i,j} - f_{i-1,j}\right)^2 + \left(f_{i-1,j+1} - f_{i-1,j}\right)^2 + \varepsilon^2}} + \frac{f_{i,j} - f_{i,j-1}}{\sqrt{\left(f_{i+1,j-1} - f_{i,j-1}\right)^2 + \left(f_{i,j} - f_{i,j-1}\right)^2 + \varepsilon^2}} - \frac{f_{i+1,j} + f_{i,j+1} - 2f_{i,j}}{\sqrt{\left(f_{i+1,j} - f_{i,j}\right)^2 + \left(f_{i,j+1} - f_{i,j}\right)^2 + \varepsilon^2}}. \tag{7}$$

The number of iterations of ART_TV was varied in three steps 10, 30 and 90.

2.2 Computer simulation

Figure 1 shows the object (Shepp–Logan phantom) used for the computer simulation. White noise with mean 0 and standard deviation 10 was added to the object according to the Gaussian probability density function, and the sinogram was obtained by Radon transform. The maximum signal intensity of the object was 100, and the matrix size was 256 × 256. The bias–noise curve for the reconstructed images was evaluated [21]. The metrics were calculated as

$$\text{Bias} = \sqrt{\frac{\sum_j \left(q_j - r_j\right)^2}{M}}, \tag{8}$$

$$\text{Noise} = \sqrt{\frac{\sum_j \left(x_j - q_j\right)^2}{M}}, \tag{9}$$

where M is the number of pixels in the image, q the reconstructed image without noise, r the object image, and x the reconstructed image with noise. The estimations were carried out 10 times, and the mean values were calculated.

2.3 Phantom studies with a commercially available MRI system

To compare ART_TV with the FT experimentally, we first imaged a quality-control phantom (5128754 Rev7, AllParts MEDICAL, Nashville, USA). The phantom was made of acrylic and filled with distilled water. The phantom included a series of rectangular waves and a disk region (Fig. 2). The scanning parameters were as follows: pulse sequence, TrueFISP; trajectory of k-space, radial; TR/TE, 11.8/5.9 ms; flip angle, 70°; FOV, 120 × 120 mm^2; base matrix size, 256; number of views, 256; slice thickness, 10 mm; bandwidth, 130 Hz/pixel. The parallel imaging technique was not used; a single-channel flex coil was used. The scan was repeated

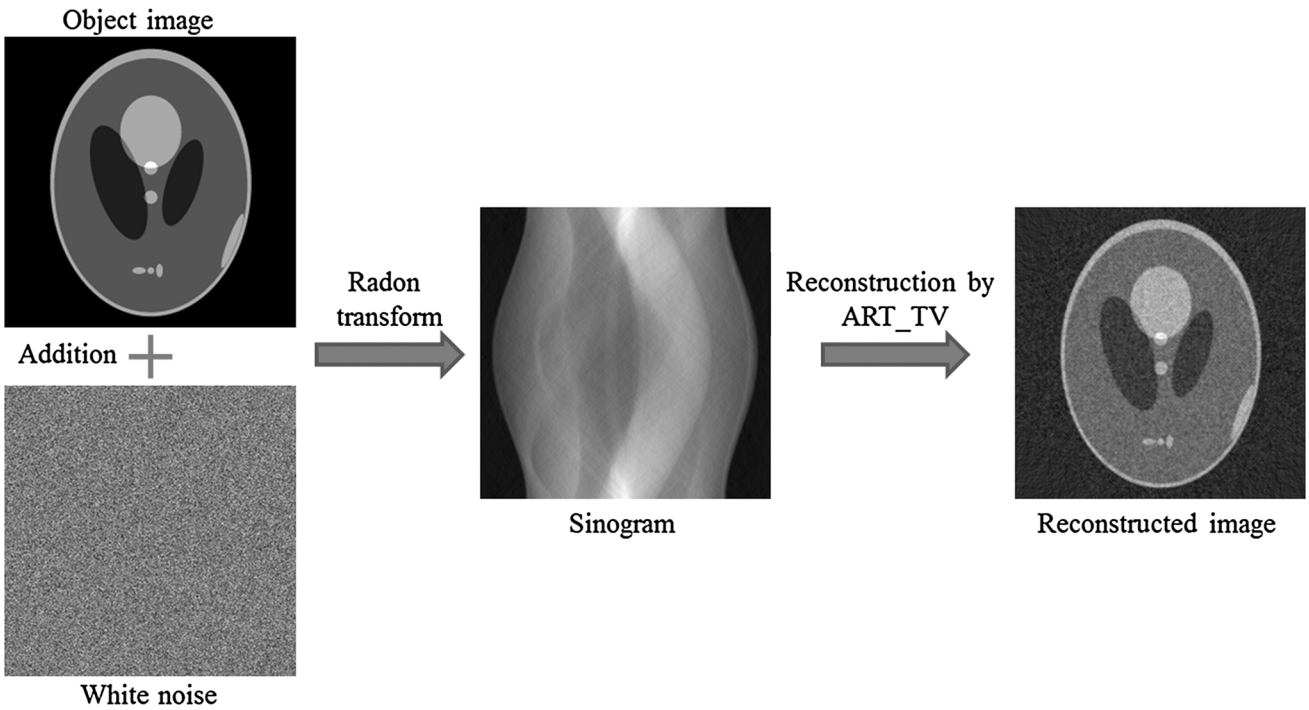

Fig. 1 Process of numerical simulation. Noise with a Gaussian probability density function was added to the object (Shepp–Logan phantom), and a sinogram was obtained by Radon transform. The *line* integral along the *straight line* connected pixel (*i, j*) and the detector. The sinogram was reconstructed by ART_TV to yield the evaluation images

10 times so as to avoid sources of measurement errors such as signal inhomogeneity from the scanner, coil, and phantom. For the FT method, the conversion from polar data to Cartesian data was done by bilinear interpolation. The reconstruction by ART_TV was performed with the polar data. To evaluate resultant images, we drew a profile curve through the series of rectangular waves, and the modulation transfer function (MTF) was measured [22, 23]. In addition, a region of interest (ROI) was set on the disk region, and the SNR was estimated by the subtraction method [24]. The positions of the profile curve and of the ROI are shown in Fig. 2.

2.4 Investigation with use of a kiwi fruit

Our second experimental test involved scanning of a kiwi fruit. The scanning parameters were the same as for the quality-control phantom, with the exception of the FOV and the slice thickness. The new FOV was 60 × 60 mm^2, and the new slice thickness was 5 mm. Two kinds of receiver coils, a single-channel flex coil (high-SNR) and a single-channel body coil built in the MRI system (low-SNR), were employed. The influence of the iteration number and the regularization parameter, β, was investigated, and a comparison of images reconstructed by ART_TV and FT was carried out. A visual assessment of the images was performed by two technologists, each of whom had more than 10 years of experience in MRI.

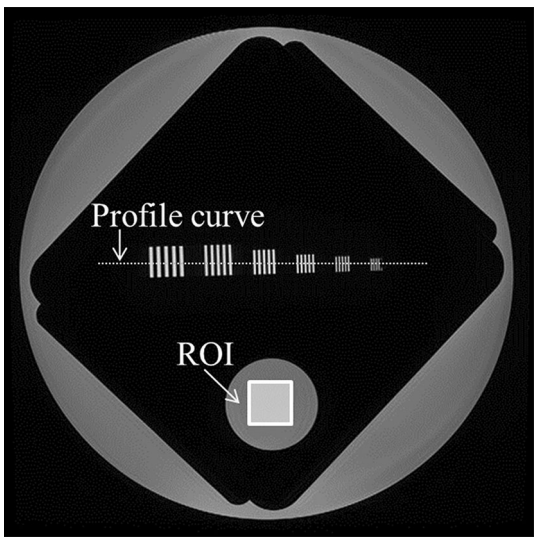

Fig. 2 The quality-control phantom included a series of rectangular-wave and a disk region. The MTF was measured on the *dotted line* across the rectangular wave, and the SNR was measured within the white square ROI

3 Results

3.1 Computer simulation

Figure 3 shows the bias–noise curve for ART_TV. As the iteration number increased, the bias decreased for all β, although the noise increased as well. Figure 4 shows the reconstructed images with $\beta = 0.01$ %. When the iteration number was 10, the image was somewhat blurred (Fig. 4a). As the iteration number increased, the image sharpened, but the noise eventually became conspicuous (Fig. 4c). Figure 5 shows the reconstructed images after 90 iterations. The largest β obscured the detail of the image, but the noise was reduced (Fig. 5c).

3.2 Experimental images of the phantom

Figure 6 shows the results for the MTF of the phantom images. The MTF improved considerably as the iteration number increased for $\beta = 0.01$ % (Fig. 6a). For $\beta = 0.1$ %, the improvement of the MTF as the number of iterations increased was smaller, as shown in Fig. 6b. For $\beta = 1$ %, the MTF was almost unchanged as the number of iterations increased (Fig. 6c).

Figure 7 shows images with $\beta = 0.01$ %. These images were obtained by enlarging the part of the main image that shows the rectangular-wave chart. After 10 iterations, the

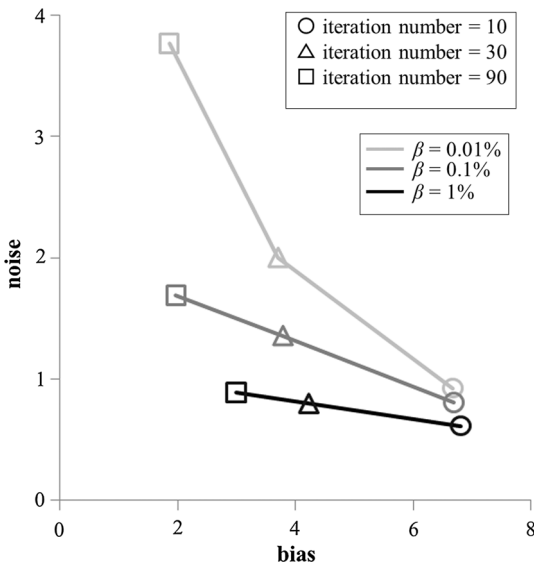

Fig. 3 Trade-off between spatial resolution and SNR ratio was investigated by the bias–noise *curve* in the computer simulations. The *vertical axis* and the *horizontal axis* represent the noise and bias, respectively. The *circles*, *triangles*, and *squares* show the number of iterations equal to 10, 30, and 90, respectively. The *light-gray*, *gray*, and *black lines* show the regularization parameter β corresponding to 0.01, 0.1, and 1 % to the maximum signal intensity of the updated image at the $m + 1$th subiteration within the kth iteration

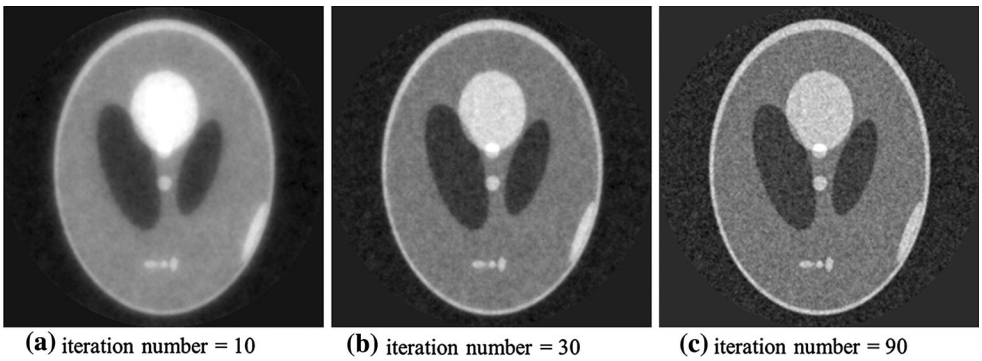

Fig. 4 Shepp–Logan phantom images reconstructed by ART_TV in each iteration with $\beta = 0.01$ %. The window level and window width are equalized on each image (this display condition also held for the other images shown in Figs. 5, 7, 8, 10, 11, 12, and 13)

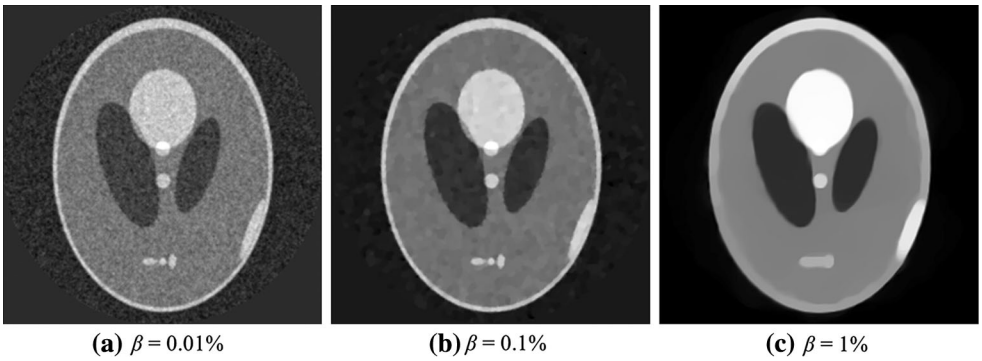

Fig. 5 Shepp–Logan phantom images reconstructed by ART_TV with use of different values of β. The number of iterations was 90

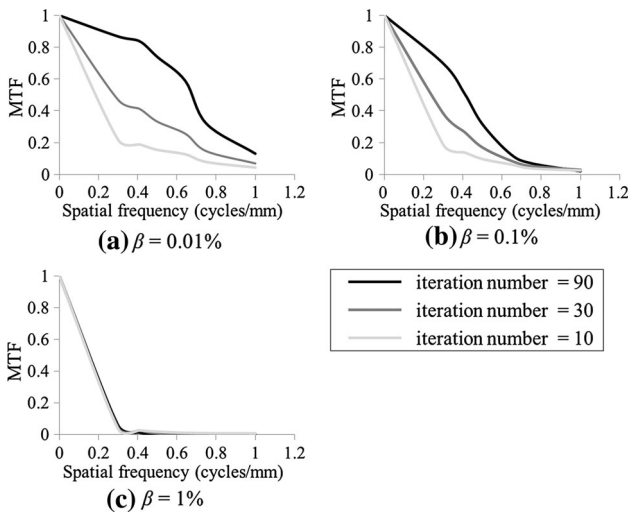

Fig. 6 Effect of β on MTF for the quality-control phantom. The *black*, *gray*, and *light-gray lines* represent the number of iterations corresponding to 90, 30, and 10, respectively

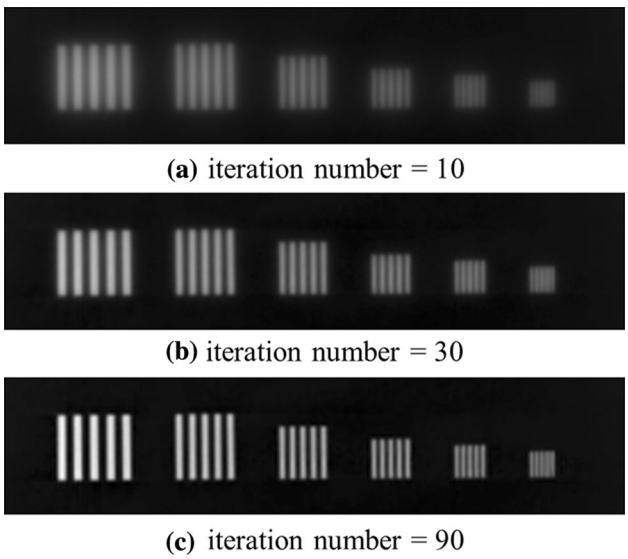

Fig. 7 Comb images reconstructed by ART_TV in each iteration with $\beta = 0.01$ %. These images are shown enlarging the part of the rectangular-wave chart at the phantom image

rectangles were blurred (Fig. 7a). As the number of iterations increased, the rectangles became sharper (Fig. 7b, c). Figure 8 compares the images obtained after 90 iterations, but with different values of β. As β increased, the rectangles were depicted less distinctly. Even if the distance between the rectangles was large enough, neighboring rectangles were almost not distinguishable for $\beta = 1$ %

(Fig. 8c). Table 1 shows the results for the SNR. The SNR improved with an increase in β, whereas it deceased with an increase in the number of iterations, irrespective of the magnitude of β.

3.3 Comparison of image reconstruction method on the basis of MTF and SNR

Figure 9 shows the MTF for ART_TV compared to that for the FT. The MTF of ART_TV was worse than that for the FT, especially for high frequencies. The upper row of Fig. 10 shows the reconstructed images of ART_TV with the iteration number 90 and $\beta = 0.01$ %, and the bottom row shows the images for the FT. Although the rectangles with small spacing were depicted more clearly with FT than with ART_TV, there was no large difference between the algorithms with regard to the delineation of the rectangles with large spacing. The SNRs of the ART_TV and FT were 56.5 ± 2.3 and 14.5 ± 0.2, respectively. Thus, the SNR of ART_TV was higher than that of the FT.

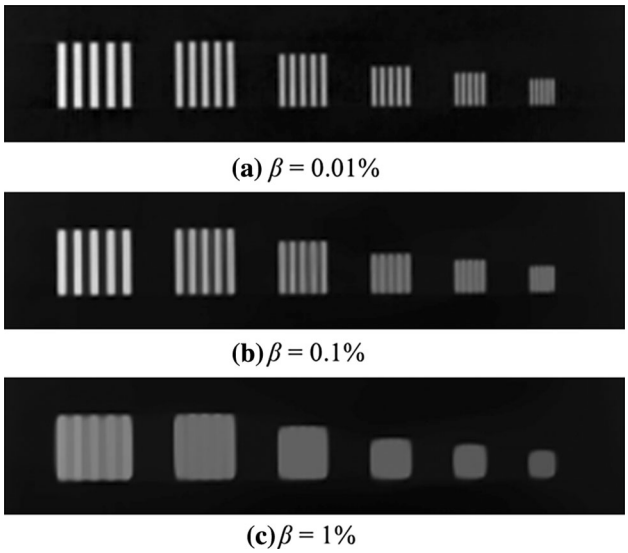

Fig. 8 Comb images reconstructed by ART_TV at each β. The number of iterations is 90. These images are shown enlarging the part of the rectangular-wave chart at the phantom image

3.4 Experimental images of a kiwi fruit

Figure 11 shows the reconstructed image of the kiwi fruit with $\beta = 0.01$ %. In the case of use of a flex coil (Fig. 11a–c), the structure of the kiwi became clearer as the iteration number increased. However, when a body coil was used, a large number of iterations reduced the image quality due to increased noise (Fig. 11d–f). Figure 12 shows the reconstructed images with the iteration number 90. The details of the kiwi fruit were obscured to some extent for $\beta = 1$ % with the flex coil (Fig. 12a–c). In the

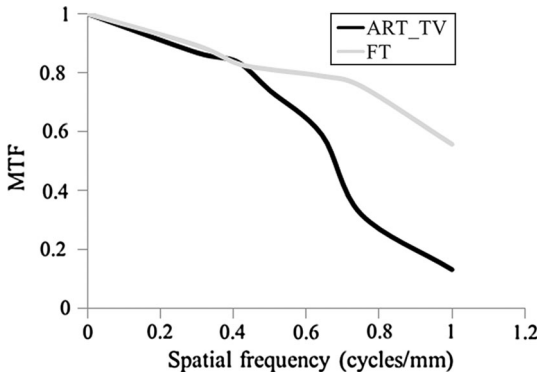

Fig. 9 Results of MTF by ART_TV and FT with the quality-control phantom. The *black* and *light-gray lines* show ART_TV and FT, respectively. In ART_TV, the number of iterations and β are 90 and 0.01 %, respectively

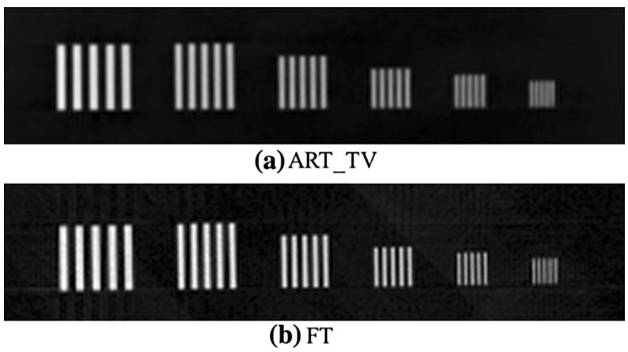

Fig. 10 Comb images reconstructed by ART_TV and FT. In ART_TV, the number of iterations and the β are 90 and 0.01 %, respectively. These images are shown enlarging the part of the rectangular-wave chart at the phantom image

Table 1 SNRs for the images of the experimental phantom as a function of the number of iterations and of β

	Iteration number = 10	Iteration number = 30	Iteration number = 90
$\beta = 0.01$ %	193.7 ± 15.9	94.5 ± 5.5	56.51 ± 2.3
$\beta = 0.1$ %	391.3 ± 89.5	349.3 ± 91.1	341.12 ± 96.1
$\beta = 1$ %	1012.3 ± 375.8	902.2 ± 334.3	890.85 ± 308.2

The values are represented as mean ± standard deviation

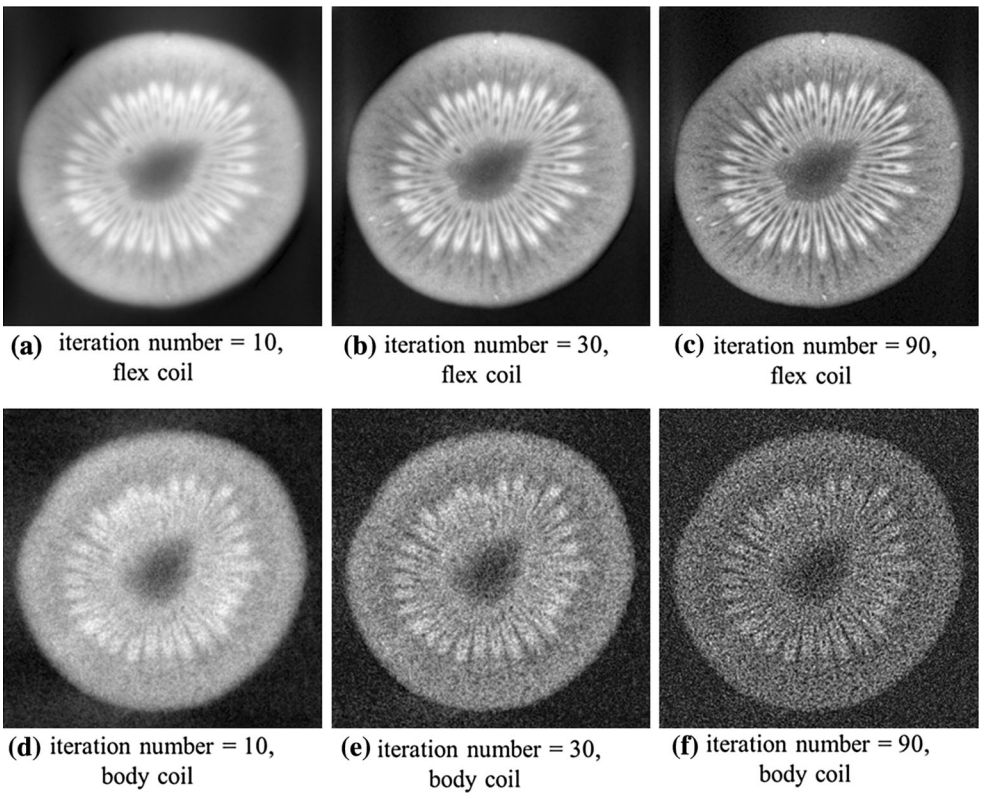

Fig. 11 Kiwi fruit images reconstructed by ART_TV at each iteration with $\beta = 0.01$ %. The *upper row* shows the images by use of a flex coil, and the *bottom row* shows those with use of a body coil

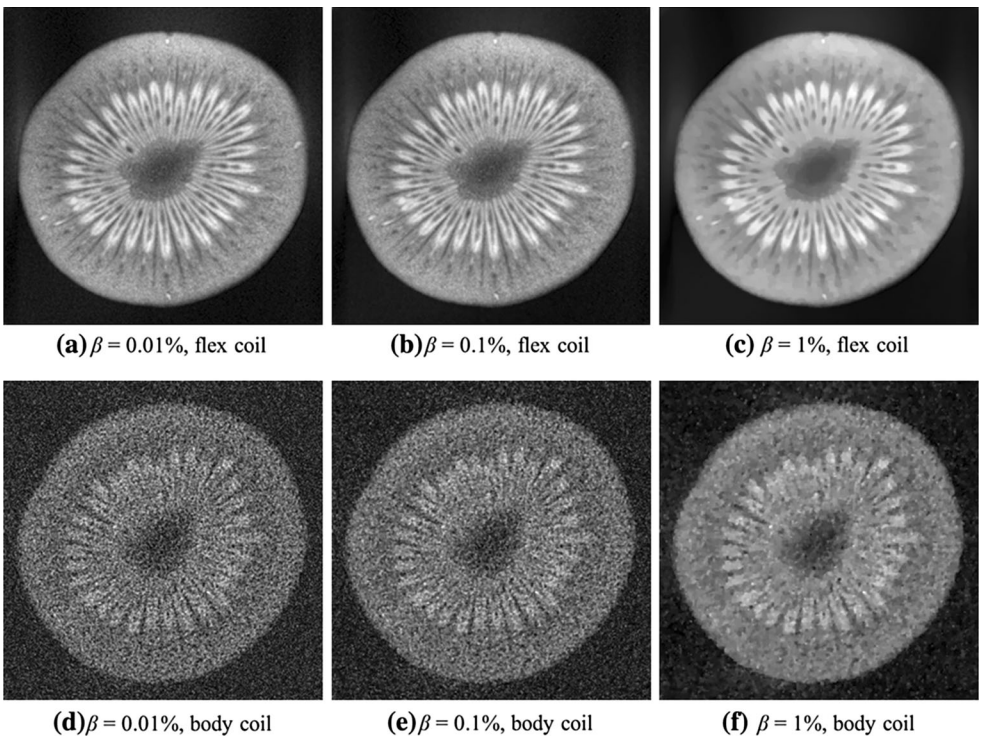

Fig. 12 Kiwi fruit images reconstructed by ART_TV at each β. The number of iterations was 90. The *upper row* shows the images by use of a flex coil, and the *bottom row* shows those with use of a body coil

case of use of a body coil (Fig. 12d–f), the noise was suppressed effectively as β was increased. Figure 13 compares the reconstructed images with ART_TV to those with the FT. For ART_TV, the number of iterations was 90 and $\beta = 0.01$ % with a flex coil (Fig. 13a), and the number was 30 and $\beta = 0.1$ % with a body coil (Fig. 13c). When the flex coil was used (Fig. 13a, b), no significant difference in image quality was observed between ART_TV and FT. However, in the case of the body coil (Fig. 13c, d), the image quality of ART_TV was better than that of the FT.

4 Discussion

ART was initially employed for SPECT and CT [25–27]. Recently, ART has been used in MRI [28, 29]. ART updates the pixel value for each projection in angular-view sampling. When all projection data are used for updating of the image, one iteration has been accomplished. If noise is absent and a global minimum for the objective function exists, the updated image gradually becomes approximated to the object image as the iteration number increases. However, if noise is present, there is an inconsistency between object and projection data, and noise amplification occurs with an increase in the iteration number, so that the reconstructed image degrades even if a regularization term has been included in the objective function that is being optimized. Thus, choosing the best regularization parameter and then stopping the iterations at the optimum time are critical in ART_TV.

TV regularization works satisfactorily for reconstruction of the image with piecewise constant and its ability to reduce noise without loss of edge sharpness is good, provided the object consists of areas with constant values as does the Shepp–Logan phantom. If the object has a more complicated texture such as in the case of a kiwi fruit, the trade-off between noise reduction and the preservation of internal structure presents a difficult choice, in contrast to the case for the Shepp–Logan phantom.

In the present work, the kiwi fruit was reconstructed satisfactorily, as judged by visual impression with ART_TV by use of 90 iterations and $\beta = 0.01$ % for a flex coil that has a high SNR, but for the body coil a smaller number of iterations and a larger β are required. Because β was determined by the maximum value of the iterative reconstructed image, the optimal β depends on the scan condition affecting the SNR of the reconstructed image. In the present work, the upper limit of the number of iterations was set at 90. This choice was made on the basis of the trade-off between the bias and noise in the simulation study with the Shepp–Logan phantom. Furthermore, β was tentatively assigned to be in the range of 0.01–1 %. We consider that the β used in the present work is not necessarily the optimal value for other objects; therefore, further studies are necessary for determination of the optimal number of iterations and of the regularization parameter β. We anticipate carrying out such studies in the future.

When the MTF is measured in MRI, there are problems such as loss of linearity due to the modulus operation [30, 31]. For overcoming these problems, various measurement techniques have been proposed [30, 31]. In the case of a performance evaluation of an MRI device, these techniques should be employed. However, in the present work, the MTF was measured by use of a rectangular-wave chart, because we focused on the comparison of the MTF for different image reconstruction methods.

Computationally, ART_TV reconstruction is much more demanding than FT reconstruction. The reconstruction time for the FT was 4 s; on the other hand, that of ART_TV after 90 iterations was about 1000 s. Reduction of the calculation cost is a goal for ART_TV. For achieving this goal, an acceleration method using GPU (graphics processing unit) hardware can be expected [32]. The evolution toward high-speed computing might achieve that in the future.

In this study, the result of the image reconstruction by the ART_TV has converged without diverging. However, clinical data were not used in this study. Thus, it is

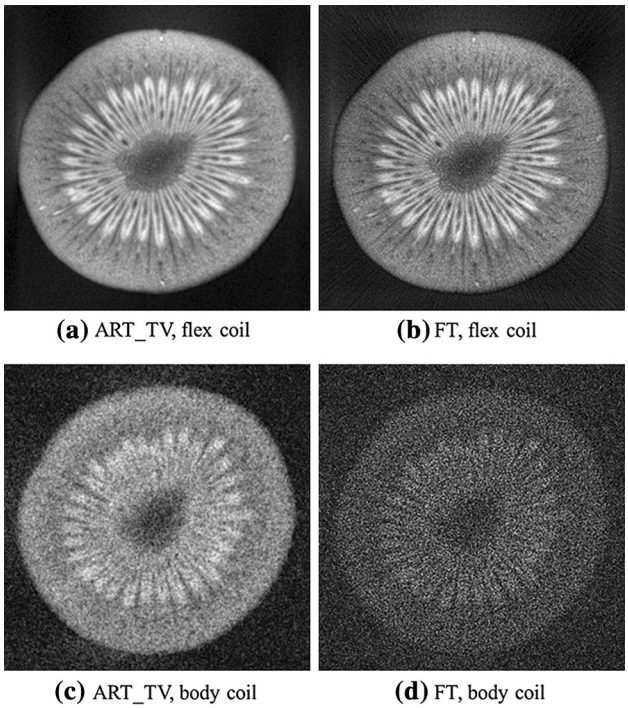

Fig. 13 Kiwi fruit images reconstructed by ART_TV and FT. The *upper row* shows the images by use of a flex coil, and the *bottom row* shows those with use of a body coil. The number of iterations and the β of ART_TV with a flex coil were 90 and 0.01 %, and those with a body coil were 30 and 0.1 %, respectively

necessary to estimate the repeatability of ART_TV by using clinical data. In addition, quantitative analysis such as the contrast-to-noise ratio by use of the ART_TV is important, because only the SNR and visual assessment were used in this study. We consider that these investigations are one of the meaningful future tasks.

5 Conclusion

We studied the performance of the algebraic reconstruction method combined with TV regularization (ART_TV) for conventional radial MRI sampling. Both the iteration number and the regularization parameter β in ART_TV affect the image quality. For low-SNR data, visually improved image quality was achieved with ART_TV in comparison with that of the FT, if a small number of iterations and a large β were employed.

Acknowledgments This research has been supported by a Grant-in-Aid for Scientific Research (KAKENHI No. 26461832).

Conflict of interest The authors declare that they have no conflict of interest in this study.

References

1. Bergin CJ, Pauly JM, Macovski A. Lung parenchyma: projection reconstruction MR imaging. Radiology. 1991;179(3):777–81.
2. Glover GH, Pauly JM. Projection reconstruction techniques for reduction of motion effects in MRI. Magn Reson Med. 1992;28(2):275–89.
3. Song HK, Dougherty L. k-space weighted image contrast (KWIC) for contrast manipulation in projection reconstruction MRI. Magn Reson Med. 2000;44(6):825–32.
4. Gmitro AF, Kono M, Theilmann RJ, Altbach MI, Li Z, Trouard TP. Radial GRASE: implementation and applications. Magn Reson Med. 2005;53(6):1363–71.
5. Pipe JG. Reconstructing MR images from undersampled data: data-weighting considerations. Magn Reson Med. 2000;43(6):867–75.
6. Rahmer J, Börnert P, Groen J, Bos C. Three-dimensional radial ultrashort echo-time imaging with T2 adapted sampling. Magn Reson Med. 2006;55(5):1075–82.
7. Takizawa M, Ito T, Itagaki H, Takahashi T, Shimizu K, Harada J. Modified echo peak correction for radial acquisition regime (RADAR). Magn Reson Med Sci. 2009;8(4):149–58.
8. Stehning C, Börnert P, Nehrke K, Eggers H, Dössel O. Fast isotropic volumetric coronary MR angiography using free-breathing 3D radial balanced FFE acquisition. Magn Reson Med. 2004;52(1):197–203.
9. Spuentrup E, Katoh M, Buecker A, Manning WJ, Schaeffter T, Nguyen TH, Kühl HP, Stuber M, Botnar RM, Günther RW. Free-breathing 3D steady-state free precession coronary MR angiography with radial k-space sampling: comparison with Cartesian k-space sampling and cartesian gradient-echo coronary MR angiography—pilot study. Radiology. 2004;231(2):581–6.
10. Boubertakh R, Prieto C, Batchelor PG, Uribe S, Atkinson D, Eggers H, Sørensen TS, Hansen MS, Razavi RS, Schaeffter T. Whole-heart imaging using undersampled radial phase encoding (RPE) and iterative sensitivity encoding (SENSE) reconstruction. Magn Reson Med. 2009;62(5):1331–7.
11. Katoh M, Stuber M, Buecker A, Günther RW, Spuentrup E. Spin-labeling coronary MR angiography with steady-state free precession and radial k-space sampling: initial results in healthy volunteers. Radiology. 2005;236(3):1047–52.
12. Gabr RE, Aksit P, Bottomley PA, Youssef AB, Kadah YM. Deconvolution-interpolation gridding (DING): accurate reconstruction for arbitrary k-space trajectories. Magn Reson Med. 2006;56(6):1182–91.
13. Mistretta CA, Wieben O, Velikina J, Block W, Perry J, Wu Y, Johnson K, Wu Y. Highly constrained backprojection for time-resolved MRI. Magn Reson Med. 2006;55(1):30–40.
14. Block KT, Uecker M, Frahm J. Undersampled radial MRI with multiple coils. Iterative image reconstruction using a total variation constraint. Magn Reson Med. 2007;57(6):1086–98.
15. Moriguchi H, Duerk JL. Iterative next-neighbor regridding (INNG): improved reconstruction from nonuniformly sampled k-space data using rescaled matrices. Magn Reson Med. 2004;51(2):343–52.
16. Gopi VP, Palanisamy P, Wahid KA, Babyn P. MR image reconstruction based on iterative split bregman algorithm and nonlocal total variation. Comput Math Methods Med. 2013;2013:985819.
17. Radin LI, Osher S, Fatami E. Nonlinear total variation based noise removal algorithm. Physica D. 1992;60:259–68.
18. Sidky EY, Kao CM, Pan X. Accurate image reconstruction from few-views and limited-angle data in divergent-beam CT. J X-ray Sci Tech. 2006;14(2):119–39.
19. Keeling SL, Clason C, Hintermüller M, Knoll F, Laurain A, von Winckel G. An image space approach to Cartesian based parallel MR imaging with total variation regularization. Med Image Anal. 2012;16(1):189–200.
20. He Q, Weng D, Zhou X, Ni C. Regularized iterative reconstruction for undersampled BLADE and its applications in three-point Dixon water-fat separation. Magn Reson Med. 2011;65(5):1314–25.
21. Nuyts J, De Man B, Dupont P, Defrise M, Suetens P, Mortelmans L. Iterative reconstruction for helical CT: a simulation study. Phys Med Biol. 1998;43(4):729–37.
22. Okano Y, MTF analysis and its measurements for digital still camera. In: 50th annual conference: a celebration of all imaging. Cambridge, Massachusetts; 1997. p. 383–87. http://www.imaging.org/IST/store/epub.cfm?abstrid=110.
23. Japan Society of Radiological Technology. Handbook of clinical radiological technology experiment. Tokyo: Tsushosangyokenkyusha; 1996. p. 182–9.
24. Association National Electrical Manufactures. Determination of signal-to-noise ratio (SNR) in diagnostic magnetic resonance imaging MS1-2008. Washington, DC: NEMA; 2008.
25. Koral KF, Rogers WL. Application of ART to time-coded emission tomography. Phys Med Biol. 1979;24(5):879–94.
26. Guan H, Gordon R. A projection access order for speedy convergence of ART (algebraic reconstruction technique): a multilevel scheme for computed tomography. Phys Med Biol. 1994;39(11):2005–22.
27. Guan H, Gordon R, Zhu Y. Combining various projection access schemes with the algebraic reconstruction technique for low-contrast detection in computed tomography. Phys Med Biol. 1998;43(8):2413–21.
28. Kadah YM, Hu X. Algebraic reconstruction for magnetic resonance imaging under B0 inhomogeneity. IEEE Trans Med Imaging. 1998;17(3):362–70.
29. Weiger M, Hennel F, Pruessmann KP. Sweep MRI with algebraic reconstruction. Magn Reson Med. 2010;64(6):1685–95.

30. Steckner MC, Drost DJ, Prato FS. Computing the modulation transfer function of a magnetic resonance imager. Med Phys. 1994;21(3):483–9.
31. Miyati T, Fujita H, Kasuga T, Koshida K, Sanada S, Banno T, Mase M, Yamada K. Measurements of MTF and SNR(f) using a subtraction method in MRI. Phys Med Biol. 2002;47(16):2961–72.
32. Yan G, Tian J, Zhu S, Dai Y, Qin C. Fast cone-beam CT image reconstruction using GPU hardware. J X-ray Sci Tech. 2008;16:225–34.